iScience

CellPress
OPEN ACCESS

Article

A T cell repertoire timestamp is at the core of responsiveness to CTLA-4 blockade

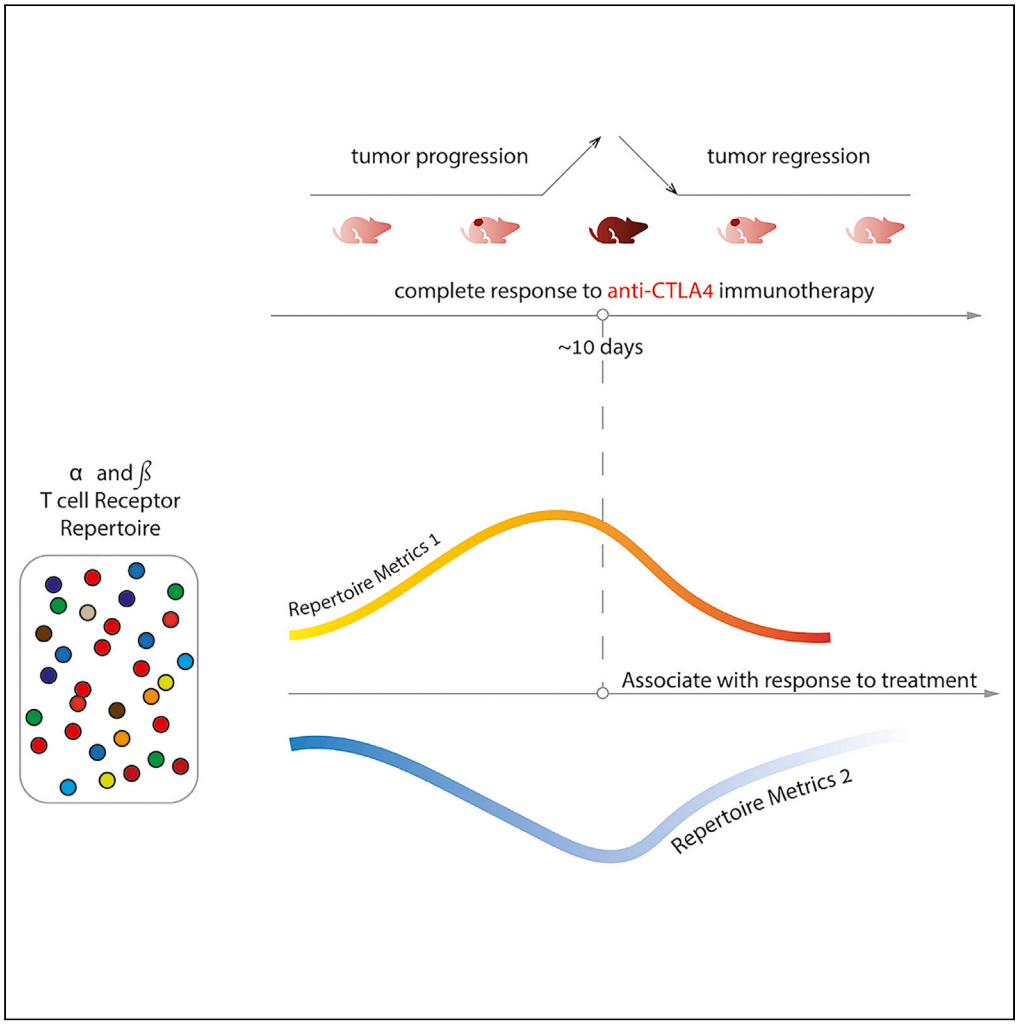

Hagit Philip, Tom Snir, Miri Gordin, Mikhail Shugay, Alona Zilberberg, Sol Efroni

sol.efroni@biu.ac.il

HIGHLIGHTS

Response to ICI is associated with pre-treatment TCR repertoire in mice

TCR repertoire goes through distinct, ICI-dependent changes with time

Tumor size and its response to ICI can be tracked by TCR repertoire metrics

A single time point is found to be a focal point of the immune response

Philip et al., iScience 24, 102100
February 19, 2021
https://doi.org/10.1016/j.isci.2021.102100

iScience

CellPress
OPEN ACCESS

Article

A T cell repertoire timestamp is at the core of responsiveness to CTLA-4 blockade

Hagit Philip,[1,3] Tom Snir,[1,3] Miri Gordin,[1] Mikhail Shugay,[2,3] Alona Zilberberg,[1] and Sol Efroni[1,4,*]

SUMMARY

Biology of the response to anti-CTLA-4 involves the dynamics of specific T cell clones. Reasons for clinical success and failure of this treatment are still largely unknown. Here, we quantified the dynamics of the T cell receptor (TCR) repertoire, throughout 4 weeks involving treatment with anti-CTLA-4, in a syngeneic mouse model for colorectal cancer. These dynamics show an initial increase in clonality in tandem with a decrease in diversity, effects which gradually subside. Furthermore, response to treatment is tightly connected to the shared and public parts of the T cell repertoire. We were able to recognize time-dependent behaviors of specific TCR sequences and cell types and to show the response is dominated by specific motifs. We see that a single, specific time point might be useful to inform a physician of the true response to treatmentThe research further highlights the importance of temporal analyses of the immune response.

INTRODUCTION

The inhibition of negative immune regulation to treat cancer is now an essential tool in the oncologist's toolbox. The cytotoxic T lymphocyte-associated antigen 4 (CTLA-4) (Leach et al., 1996; Rowshanravan et al., 2018) and programmed cell death protein 1 (PD-1) (McDermott and Jimeno, 2015; Postow et al., 2015) were the first to be targeted, whereas other receptors for antibody therapeutics are constantly being sought (Sharma et al., 2017; Tang et al., 2018). However, response rates of patients treated with the currently available drugs are not optimal, and a treating physician is left with little knowledge as to the expected course of response (Pai et al., 2019; Pallocca et al., 2019).

Importance of immune checkpoint inhibition in CRC

Recently, colorectal cancers (CRCs) were shown to be promising candidates for immunotherapy (Ganesh et al., 2019). In those cancers, the use of anti-CTLA-4 has been shown to increase the diversity and the composition of the human T cell repertoire (Cha et al., 2014). Unlike other cancer types, immunotherapy treatment of CRC shows long-term improvement and remission. This has been suggested to be linked with the central role the immune system takes in this cancer type (Galon et al., 2006, 2007). As such, immune checkpoint inhibition has been the focus of other research, with other targets such as LAG3 (Long et al., 2018), TIM3 (He et al., 2018), and TIGIT (Harjunpaa and Guillerey, 2020), which are currently tested and are in various phases of clinical trials. These findings, although mostly done in humans, led us to design a study focused on the changes that the T cell repertoire goes through over the time course during and after treatment with anti-CTLA-4.

Repertoire Sequencing in CRC

To see changes in the immune response, and especially changes that are the result of immunotherapy, it is interesting to look at repertoire sequencing (Rep-seq, Benichou et al., 2012, or AIRR-seq, Rubelt et al., 2017). Such works often include two metrics used extensively by multiple groups to quantify the T cell repertoire: diversity and clonality. The origin of these measurements is metrics used to assess and quantify populations in various ecosystems, where the plurality of species is of great importance. Diversity is a measurement that tells us of the total number of species (in this work, total number of different T cell receptors [TCRs]). Diversity in essence does not take into account the number of items (number of T cells) that belong to each species (to each T cell clone). Clonality, on the other hand, does include information regarding the

[1]The Mina & Everard Goodman Faculty of Life Sciences, Bar-Ilan University, Ramat-Gan, Israel

[2]Shemyakin-Ovchinnikov Institute of Bioorganic Chemistry, Russian Academy of Sciences, Moscow, Russia

[3]Center for Precision Genome Editing and Genetic Technologies for Biomedicine, Pirogov Russian National Research Medical University, Moscow, Russia

[3]These authors contributed equally

[4]Lead Contact

*Correspondence: sol.efroni@biu.ac.il

https://doi.org/10.1016/j.isci.2021.102100

number of items in each species (the number of T cells in each clone). Clonality is higher when a specific species includes more items (when a specific T cell clone is more abundant).

Several works focused on diversity and clonality of the TCR repertoire following immunotherapy (Beer et al., 1988; Field et al., 2017; Hosoi et al., 2018; Robert et al., 2014; Valpione et al., 2020) and all found that the expected increase in clonality and decrease in diversity often precede a critical point in treatment. Other works, such as the computational analysis of CRC performed by Cha et al. (2017) detected 1,940 distinct antibody peptides and 163 pairs of antibody peptides with a single amino acid variant that showed correlation with survival times of sick individuals. Other works focused on tumor-infiltrating lymphocytes (Treiner et al., 2003) found both in tumors and in the surrounding tissue, to study their TCR repertoire (Sherwood et al., 2013), or on sequencing tumor-draining lymph nodes (Matsuda et al., 2019) to differentiate metastasis and non-malign tissues. Recent works (Zhang et al., 2019) used single-cell RNA sequencing (scRNA-seq) to further explore the tumor-infiltrating lymphocytes of patients with CRC, whereas the TCR repertoire itself might be used as a liquid biopsy alternative (Snir and Efroni, 2020). These studies show that the research community identified the importance of quantifying the TCR repertoire of patients with CRC. These findings and their conclusions led to the work presented here.

Time-dependent analysis

Over the past few years, several works studied time-dependent changes to the TCR repertoire; Oh et al. identified stages in treatment where diversification of the TCR repertoire takes place (Oh et al., 2017), whereas other works focused on the importance of a diverse TCR repertoire to avoid adverse events following immunotherapy (Cha et al., 2014) and showed that such events often occur after a drastic change in the diversity and clonality of the TCR repertoire (Subudhi et al., 2016). Although these articles, and others like them, highlighted the importance of timing and of time-dependent analysis of the TCR repertoire, a straightforward study to follow the TCR repertoire has not yet been published, despite its translational importance.

Research motivation

Our research aims to improve the understanding of changes within the TCR repertoire in mice treated with anti-CTLA-4, with a special emphasis on the time-dependent behavior of T cells. We present evidence that highlights not only the importance of choosing the correct type of analysis performed but also the timing of sampling. We also note several cell types according to their TCR association with mucosal-associated invariant T cells (MAIT) and invariant natural killer T cells (iNKT) cells that have been previously shown to accompany the immune response in treated mice. We believe the research solidifies the importance of a time-dependent analysis of immunotherapy treatment.

RESULTS

Experiment design

To set up a system that allows the monitoring of tumor progression and tumor regression following anti-CTLA-4 checkpoint immunotherapy, in tandem with measuring the repertoire, we used the MC38 syngeneic mouse model. In an anti-tumor efficacy experiment, we used 6-week-old female C57BL/6 mice (Strain C57Bl/6NAnNCrl, Charles River). Freshly cultured MC38 tumor cells (10^6 in 100μL PBS) were implanted subcutaneously into the left flank of all animals. Following implantation, primary tumor volume was determined daily by caliper measurement using the formula $W^2 \times L/2$ (L = length and W = the perpendicular width of the tumor, L > W). Eight days after tumor inoculation, mice were randomized into groups of 15 mice in the anti-CTLA-4 treatment group and 5 mice in control (untreated) group (day 0). Animals were treated intravenously on days 1, 3, and 6 starting on the day of randomization. Vehicle control animals were treated with 10 mL/kg body weight PBS. Blood samples were collected on days 0, 7, 14, and 21 (Figure 1). A total of 4 × 20 = 80 blood samples were taken throughout the experiment, and tumor (4 samples) and spleen (20 samples) were taken at the end of the experiment. We isolated peripheral blood mononuclear cells (PBMCs) by density gradient centrifugation. Library preparation and next-generation sequencing of the repertoire were performed as previously described (Rosati et al., 2017). Briefly, 100 μL blood was spun down and pellets were further processed and lysed with ACK buffer to remove erythrocytes. The resulting PBMCs, tumors, and spleens were processed for their RNA contents. 125 μg from each RNA was applied to ĆSMARTer-Mouse-TCR-Profiling-Kit (Clontech) to obtain DNA libraries, which we then sequenced using Illumine MiSeq (v3 kit). We analyzed the obtained reads for their Rep-seq data using MiXCR (Bolotin

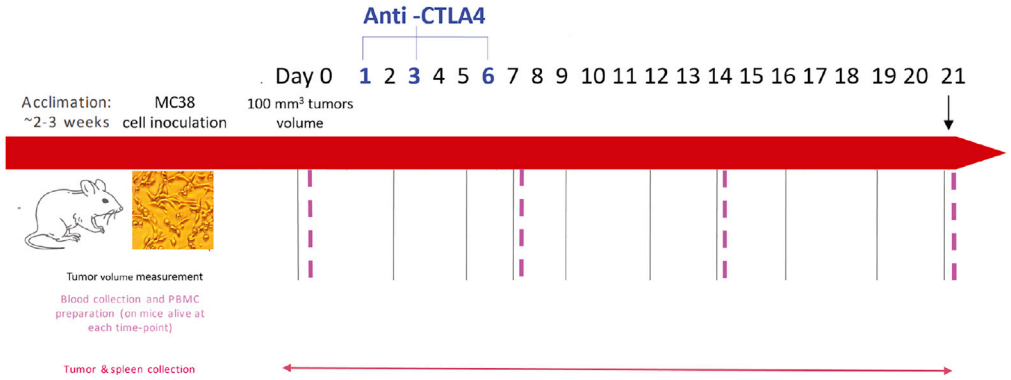

Figure 1. Experimental workflow

C57BL/6 mice were implanted with freshly cultured MC38 colon tumor cells. One group (red arrow, horizontal, 15 mice) was treated with the anti-CTLA-4 clone 9H10 on days 1, 3, and 6, whereas the control group (5 mice) remained untreated. We have drawn blood samples once a week, starting day 0, during a period of 3 weeks (purple vertical lines). From these blood samples, we obtained PBMCs and processed their RNA to produce TCR repertoire sequencing. In addition, tumor (when available) and spleen samples were collected with animal sacrifice at the termination of the experiment. Tumor volumes were measured on days 0, 2, 5, 7, 9, 12, 14, 16, 19, and 21 (black vertical lines in the figure).

et al., 2015). This workflow provided us with TCR repertoire data for all samples. As is known for the specific anti-CTLA-4 antibody clone we used (9H10), all mice responded to treatment (see also Simpson et al., 2013).

Changes in clonality and diversity are detectable at weekly sampling resolution and subside over time

Human studies showed that treatment with anti-CTLA-4 caused expansion of specific clones (Friese et al., 2020). To examine this phenomenon, we measured changes in tumor size, T cell clonality, and diversity in each mouse, in each time point (Figures 2A–2C). As expected, only treated mice showed a decrease in tumor size as their tumors receded (not all control mice lived to day 21). To study diversity, a population size metric that is often informative in repertoire analyses (see Transparent Methods), we calculated the inverse Simpson index of the TCR repertoire in alpha chain in each animal in each time point. We found that in treated mice, beta-chain diversity decreased significantly in day 7 (D7), and then gradually increased in D14 and D21 (Figure 2B). Diversity is inversely correlated to clonality (Figure 2C). When we quantified clonality in each mouse, we noticed a clear difference between the response rate in mice with low clonality (clonality <0.034) and mice with high clonality (clonality >0.034); mice with higher levels of clonality reacted faster to the treatment, and with better final outcome (e.g., a smaller tumor size) (Figure 2D). The same phenomenon in the clonality was observed in alpha chain measurements (Figures S1A–S1C).

The control group did not display significant variability in its response throughout the experiment, whereas treated mice showed a significant increase in the frequency of the 10 most abundant clones in beta chain (Figure 2E). These changes are most noticeable in D7 compared with other time points. The same observation was seen in alpha chain measurements (Figure S1D). Such changes were not found in the control group, suggesting that there are specific clones relevant to the disease in question that could be linked to the response to treatment.

These results suggest that treatment with anti-CTLA-4 leads to an expansion of some clones and to the contraction of others, leading to an increase in clonality and a decrease in diversity at the time point immediately following treatment (D7 here). As different sample sizes usually create an incomplete representation of the repertoires, we examined the 10 most expanded clones in each sample (the assumption is that even though the number of sampled CDR3 sequences is different between samples, the top clones remain at the top). To quantify these changes within the top 10 clones, we used D0 as a baseline. That is, we divided the clonal frequencies obtained in D7, 14, and 21 with that of D0. In Figure 2F we show these fold differences in the clones as they appear in four groups: the control group and three other groups that were obtained from the treated group. Full explanation of the three groups is in the Transparent Methods section. Briefly, the names "early," "mid," and "late" stand, respectively, for the animals that responded early to anti-CTLA-4

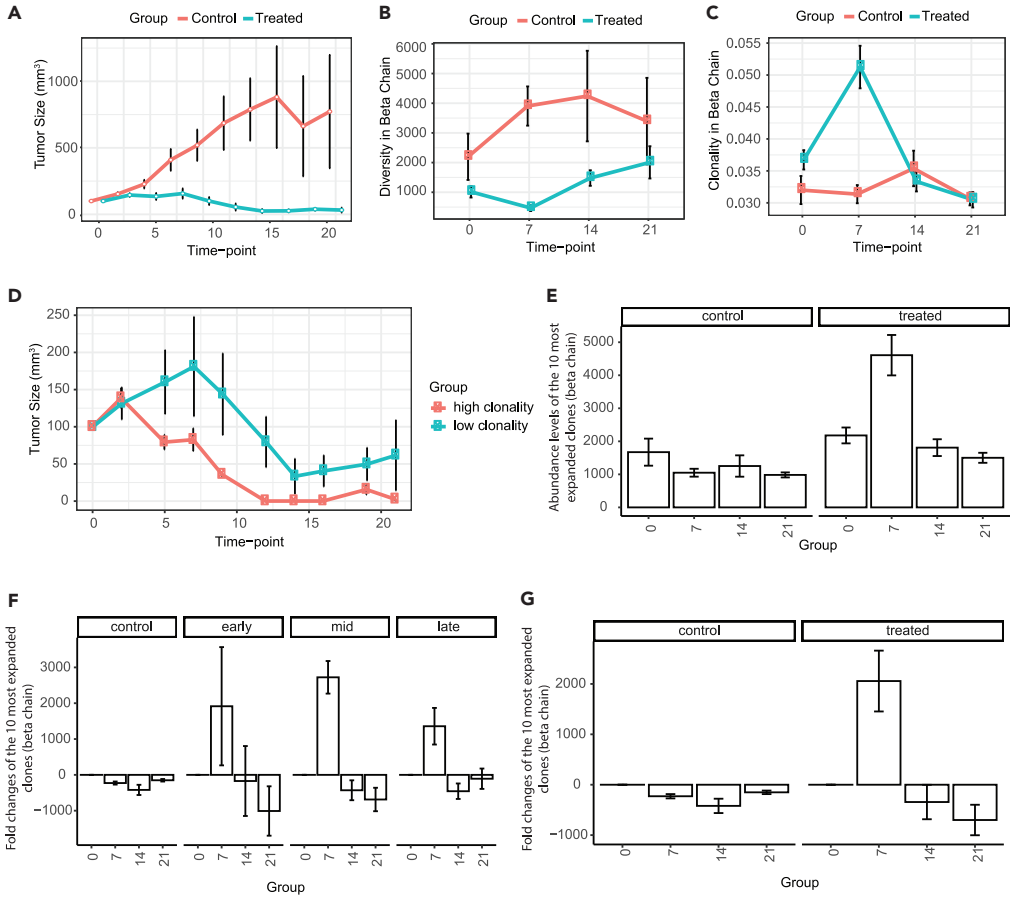

Figure 2. Changes in clonality and diversity subside over time and are distinctive to different response groups

(A–C) Changes over time in tumor size (See also Table S1) (A), diversity index for beta chain (B), and clonality index for beta chain (C) in the control group and in the treated group.

(D) Changes over time in the average tumor size. The treated mice in this panel are divided into two groups, according to their clonality index—low clonality (blue lines) and high clonality (orange lines).

(E) The abundance levels (copy number) of the 10 most expanded clones in the control and treated groups in an amino acid view, in beta chain.

(F and G) (F) Fold changes of the 10 most abundant clones in the different response groups (early, mid, late, see text) and (G) combined.

See also Figure S1. Data of all panels are represented as mean ± SEM.

treatment; the animals that responded later to treatment, and the animals that responded much later to treatment. See quantification in Transparent Methods. As seen in the figure, the response groups differ among themselves in their clonal behavior but differ greatly from the control group. This is averaged in Figure 2G, which clearly demonstrates an expansion of the dominant clones at D7, post-treatment. This expansion is absent from the control group. We can see the same behavior we discussed earlier—the only time point that demonstrates a significant increase in the top 10 clones is D7. Additionally, we see that whereas the control group presents a mostly constant abundance of the top 10 clones, the treated group experiences significant expansion of clones in D7. The same observations were also found in the alpha chain analysis (Figures S2E and S2F).

Repertoire-based stratification of mice is associated with response to treatment

We looked at the response to checkpoint inhibition treatment and its association with the identity of the T cell clones specific to each animal pre- and post-treatment. Here, we see a correlation between the abundance of public clones (clones that are shared between mice, see Transparent Methods for definition) and response to treatment. We also see a correlation between the response and the level of convergent

recombination (CR) (Smyth et al., 2000), the phenomena in which different nucleotide sequences code for the same amino acid sequence. Identical TCRα or TCRβ amino acid (Harjunpaa and Guillerey) sequences originate from different nucleotide (Pallocca et al., 2019) sequences (Quigley et al., 2010).

T cell repertoire work often discusses two types of clones: Private and Public (Venturi et al., 2008) (Li et al., 2012). Private clonotypes are tagged as such if their CDR3 (amino acid) sequences appear in only one animal in the study; Public clonotypes are tagged as such if they appear in more than one animal. We further divide Public clonotypes into two subgroups as done before (Covacu et al., 2016); we define clonotypes as Public Inclusive if they appear in more than one phenotype group of mice and Public Exclusive if they are shared only within their own phenotype group. We found that the frequency of Public Exclusive clones is fundamentally different in treated mice (all three groups, early, mid, late) from that of the control group, that is, the treated groups have a relatively higher portion of clones that are shared only within the same group. Starting at D7 (Figure 3A), these differences are most apparent from the contrast between the control group and the early-responders. The differences between the Control group and mid, early, and late can be further seen at D21 (t test: $p < 2.1 \times 10^{-5}$; $p < 1.8 \times 10^{-4}$; $p < 8.2 \times 10^{-4}$, respectively). Early-responders further show a significant increase in their frequency from D0 to D21 (t test: $p < 0.0014$). Early- and mid-responders show a significant increase between D14 and D21 (t test: $p < 5.1 \times 10^{-4}$; $p < 0.0082$, respectively). In addition, early-responders demonstrate the highest level of Public Exclusive sequences immediately after treatment, suggesting that this set of clones may be instrumental to the response.

To quantify the similarities between samples, we calculated the number of sequences shared between sample pairs. To do that, we used the 100 most abundant clones and "Morisita's index" (Rempala and Seweryn, 2013) to calculate the overlap. An analysis of alpha chains did not show higher levels of overlaps between samples within the same animal (Figure S2A). However, an analysis of the beta chain demonstrated a distinct higher overlap within samples from the same animal (Figure 3B). Quantification of the overlaps between and within the different response groups (Figure 3C) demonstrates that the control group shares a relatively lower overlap with all treated groups. For example, the overlap between control and early-responders is lower than the overlap between mid-responders and early-responders' samples (0.1541 and 0.1572, respectively, $p < 0.013$). Also interesting is the fact that samples within response groups share similar repertoires.

CR has been shown to behave differently under different conditions (Venturi et al., 2008) (Quigley et al., 2010). We, and others, have shown that an increase in CR levels correlates with an increase in sharing levels (sharing level is simply measured as the number of animals sharing a specific sequence) (Figure S2B). In the temporal behavior we report here, early-responders show a post-treatment (D7) reduction in CR levels compared with all three other groups (control, mid-responders, and late-responders). In the other groups, D7 CR levels increased (Figures S2C and S2D). When we compared the CR levels of control and treated groups, we identified a significant difference in D14 (Figures 3D and S2E). As T cells do not go through *in vivo* mutations, the increase in CR could mean either a thymic-based activity that increases in response to a peptide presented in the thymus, or, alternatively, an increase in the peripheral abundance of multiple T cell clones directed at the same peptide. Such an increase would lead to higher detection within sampling of the observed repertoire.

Network analysis of clones

The network structure of the relationships between clones is useful in visualizing and learning about the T cell repertoire. Here, we created a network representation of the top 100 clones and their abundance. To do that, we looked at the unique set of the 100 most abundant clones in each sample (this set includes ~3,200 sequences). We used this set to create a network in which the clones themselves are nodes, whose sizes are determined by the abundance of each clone. The clone size is normalized within mice; that is, for each mouse, we calculated the relative abundance of a clone compared with its frequencies in all other time points of the same mouse. Edges between nodes appear when the editing distance between sequences, calculated as Levenshtein distance, is 2 or smaller. We cluster sequences into groups of sequences with high similarity. Figure 4 shows the networks of these TCR sequences, such that every row represents the repertoires of control mice, early-responders, and late-responders, over time (time progresses from left to right). The represented network is that of the complete set of 3,200 sequences. For each sample, only sequences that appear in the sample are highlighted, with their frequency represented by node sizes

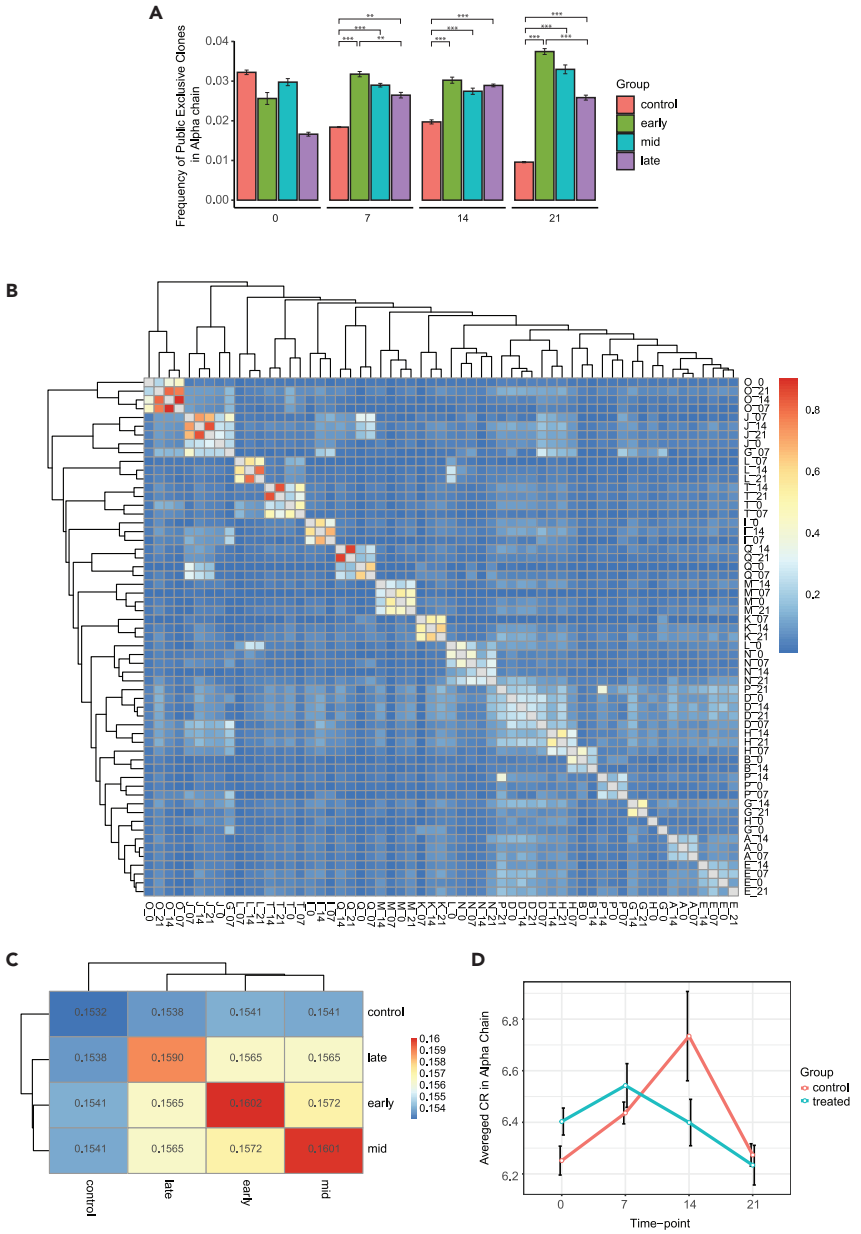

Figure 3. Repertoire-dependent response to treatment

(A) Frequency of Public Exclusive clones in each of the response groups over time. Data are presented as means ± SEM (*p < 0.05, **p < 0.01, ***p < 0.001; Student's t test). For the sake of legibility, the panel highlights a small set of some of the significant differences between the different levels. There are many additional significant contrasts.

(B) Overlaps between samples. We used the 100 most abundant beta chain clones in each sample for the calculation. The metric we used is Morisita's index (see text). The panel highlights inner similarities within samples from the same animal.

(C) The average overlap within and between groups. Each rectangle represents the average number of overlaps within all samples in a specific combination. To calculate an average overlap, we used the average over all sample combinations between two groups.

(D) Changes, over time, in the averaged CR levels in the control (Rubelt et al.) and treated (blue) groups. Data are presented as means ± SEM. The panel indicates the significant increase in CR in the treated group at D14, in contrast with the significant decrease in CR in the control group on the same day. Interestingly, the curves meet at D21.

See also figure S2.

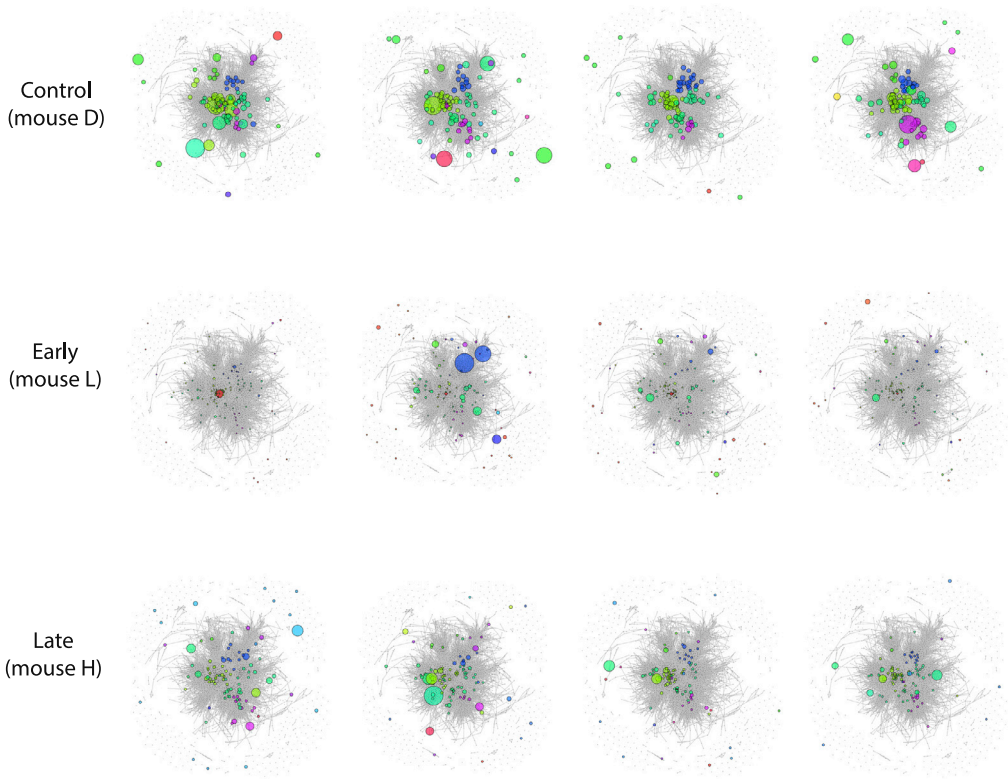

Figure 4. Network analysis of clones

Networks of a set of sequences assembled by collecting the 100 most abundant clones in each sample. Three different groups are visualized (mouse D = control; mouse L = early-responders; mouse H = late-responders). For each mouse, we see progress in time from left to right. The leftmost network is D0, whereas the rightmost network is D21. The size of the node represents the relative abundance of a clone within a mouse. We connected and clustered AA sequences according to their Levenshtein distance. An edge between two nodes appears when the distance is smaller or equal to 2.

and with clusters associated through color. The figure shows that early-responders follow a different longitudinal behavior. Specifically, in D7, where the control and late-responders' networks demonstrate a constant longitudinal behavior, with multiple high-frequency clones, the early-responders show several large clones. This D7 behavior suggests that these are the clone clusters that provide better protection, or that respond better to anti-CTLA-4, for this group of mice.

Response and behavior are related to presence of specific TCRs

Finally, we identified specific TCRs, whose sequences are associated with iNKT and MAIT. These sequences demonstrated time-dependent behavior across all phenotypes (Figure 5). iNKT cells were previously reported in the human blood pool, comprising 0.01%–1% of PBMCs (Gumperz et al., 2002), and were categorized as important immunoregulatory cells (Kronenberg, 2014; Van Rhijn and Moody, 2015). iNKT cells are some of the first cells to respond during an infection. Pre-clinical mouse studies have clearly demonstrated that iNKT cells play a critical role in tumor immunosurveillance (Smyth et al., 2000). Figure 5A shows that iNKT cells behave in a time-dependent manner in the four response groups. Interestingly, the reduction in iNKT levels from D7 to D14 is in all the treated groups (this is different from MAIT cell behavior, see Figure 5B and further discussion below) and is less significant in the control group. It is not possible to see any relevant behavior if we are not looking at the abundance of clones, but instead look only at the set of unique clones (Figure S3A). When we looked at the abundance of iNKT cells (from spleens) we identified a significant difference between treated and control mice (Figure 5C).

MAIT cells (Treiner et al., 2003), were previously reported as an abundant population in humans, where they represent up to 10% of blood T cells, whereas their role in immunity remains unclear (Godfrey et al., 2019). Despite their similarities, there are some striking differences between iNKT cells and MAIT cells; for example, most mouse MAIT cells produce the cytokine IL-17A, and only a small subset of these cells

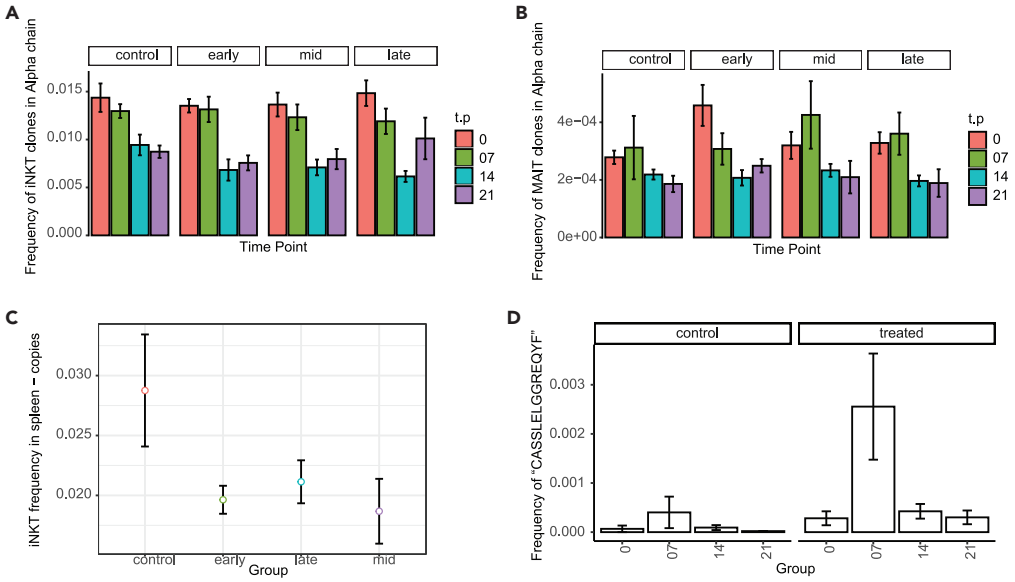

Figure 5. Response and behavior are related to the presence of specific TCRs and cell types

(A) The frequency of iNKT cells in alpha chain for all four different groups.

(B) The frequency of MAIT cells in alpha chain.

(C) The frequency iNKT cells in spleen samples in control and treated mice.

(D) The frequency of CASSLELGGREQYF (the most shared clone observed, see Table S2) in the different groups. Data of all panels are represented as mean ± SEM.

See also Figure S3.

produces the cytokine IFN-γ, whereas the opposite is true for iNKT cells. (Furthermore, in mice, iNKT cells outnumber MAIT cells 10- to 100-fold in most tissues, whereas the opposite applies for humans (Godfrey et al., 2019)). Figure 5B demonstrates how MAIT clone expansion is associated with response to immunotherapy. Although the unique repertoire of MAIT sequences did not show any significant difference (Figure S3B), MAIT abundance was higher at D0 in the group we identified as early-responders; they were significantly low in the mid-responders as well as in the late-responders. MAIT frequency does eventually go up post-treatment in those two groups. It may be that this initial abundance of MAIT cells in these specific animals is the reason they shared early response.

To identify a specific dominant group of clones, we isolated the set of clones that are within the 100 most abundant clones in D7 (which we previously identified as critical in the response) and that are shared between at least two time points of the same animal. Table S2 gives the list of 18 clones that we identified in this way in the treated mice. The sequence in the first line of the table is shared between seven of the treated mice (Figure 5D).

T cell repertoire annotation and motif discovery

We applied the TCRnet analysis as previously used to discover motifs in TCR sequencing data; this method is used to discover groups of homologous TCR sequences that are unlikely to be observed by chance and therefore are a result of antigen-driven expansion (Pogorelyy and Shugay, 2019; Ritvo et al., 2018). Our results indicate the presence of several large groups of TCR clonotypes having similar TCR sequences for both alpha and beta TCR chains. By treating repertoire as a set of homologous TCR clusters, we were able to profile the behavior of TCR groups that are likely to target the same antigen. These groups display a characteristic behavior with T cell abundance peaking at D7, and we were able to identify conserved CDR3 sequence motifs characteristic for TCR groups displaying the most prominent change in abundance.

DISCUSSION

The experiments undertaken in this article were designed to characterize the dynamics of the T cell repertoire in mice treated with anti-CTLA. The results led us to discover that the repertoire is translatable into important metrics and to discover the importance of the frequency of sampling during treatment.

Response to immunotherapy treatment is difficult to quantify, mostly because multiple factors control this response. In the experiments we described earlier, we have indeed seen the animals go through different disease courses. We have seen varying responsiveness to immunotherapy treatment, even though the mice are of identical genetic background. All treated mice eventually eliminated the tumors, but to do so, they went through major differences in their tumor volumes. What we show here, is that by measuring the T cells' repertoire clonality, diversity, and other metrics relevant to the immune response, we identified time point D7 as the one time point that informed of significant differences in future responses. Although an increase in clonality might be expected, we show that this clonality might be completely overlooked if the measurement is taken too soon, or too late.

In addition, the pathological display of changes in the disease, in this case the tumor size as it has been measured in animals, and the display of changes to the quantified behavior of the immune system, through changes in the repertoire, do not appear simultaneously, but at different times. This detachment between the two metrics adds to the importance of placing our attention over the correct temporal behavior.

We show, through network analysis of the dynamics of available TCRs and their sequence similarities, that connections between clones increase and decrease with time. These emergent networks show an association between clones and the general rate of response to treatment.

We then look at Public (shared between multiple animals) and Private (unique to one animal) clones, where we see that among the Public clones, a subset of clones that we termed "Exclusive," as they are exclusive to a specific phenotype, are expanded within the group of early-responders, over the 4 weeks duration of the experiment; This expansion is in stark contrast to the behavior of clones that are exclusive to the control group. The Control-Exclusive clones diminish over time, perhaps as they are not boosted (unlike the treated groups) by immunotherapy (Figure 3A).

We further identified unique cell types and followed their dynamics throughout the experiment. Recent articles showed the importance of MAIT cells in response to immunotherapy treatment. Here, we see that the MAIT cells we identified out of the repertoire were tightly connected to drug response (Figure 5B). It could be that these cells are influenced directly by the drug itself. In a similar manner, and following the interest in iNKT cells and their involvement with cancer response (Patel et al., 2020; Yamashita et al., 2018), we see that TCR repertoire data identifies iNKT cells in a manner that shows expansion of iNKT clones in response to treatment. Specifically, this expansion is in D0 and D7, making iNKT cells first responders to the tumor. The expansion pattern changes in D14 through 21, but it does not change in the group of mice that responded late. Interestingly, the drop in iNKT clone sizes from D7 to D14 is unique to the treated mice groups, and is less significant in the control group. If we do not look at clone sizes, but instead only at clone lists (that is, without registering their abundance) the effect disappears (Figure 5A). Also, when we studied iNKT cells in spleens of treated and of untreated mice, we saw a major difference in their abundance (Figure 5C).

We used motif discovery to identify group of TCR sequences whose expansion is driven by antigens. As Figure 6 shows, both TCR alpha and TCR beta represent such clonotypes. We can see the temporal behavior of the clonotypes identified in Figure 6, and in Figure S4. As the figure indicates, the clonotypes demonstrate extensive expansion in the treated group at D7. That expansion is missing from the control group, which means it is driven by the treatment. Furthermore, this behavior is not homogeneous across all treated mice, but rather is more apparent in a subset of treated animals. Finally, motif analysis showed the presence of several large groups of TCR clonotypes, with similar TCR sequences for both alpha and beta TCR chains. These groups peak at D7 and include conserved CDR3 motifs most likely involved in the immune response. We intend to further explore this venue of results.

Together, we present strong evidence that the timing and response to immunotherapy are connected to metrics available from the T cell repertoire. Within that general term, the T cell repertoire, we see specific behaviors in the days surrounding a specific time point, which in this experiment is D7, and which

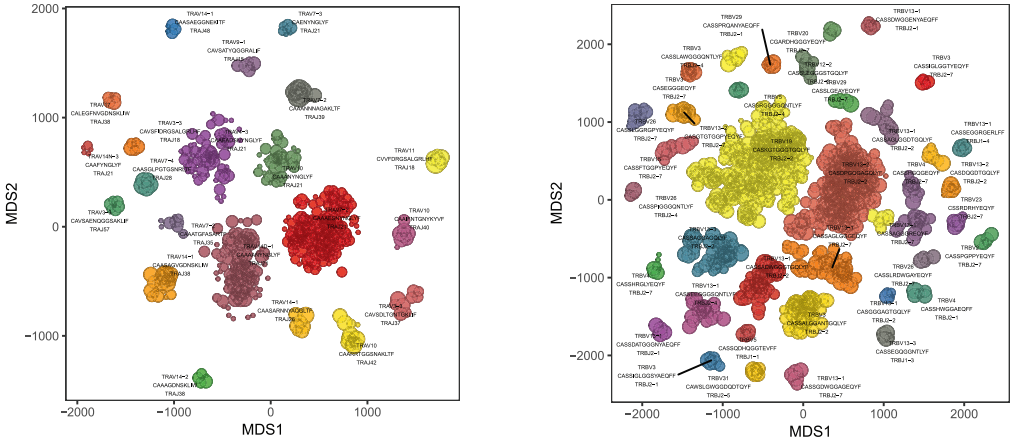

Figure 6. Cluster of clone abundance

Both TCR alpha (left) and TCR beta (right) show differences in clone sizes.

See also Figure S4.

undoubtedly calls for specificity in different settings of different tumors and different treatments. We also see specific behavior of clonal networks, clonal sharing, and iNKT and MAIT cells. Further research is needed to identify more T cells and TCR sequences involved in the immune response to the types of cancer covered here, updating personalized cancer therapy with another layer of information to be used in decision-making. We believe that this research should lead to research in human samples and in clinical settings, to allow physicians access to the temporal behavior of the immune response. This knowledge might help physicians make well-informed decisions regarding treatment choices. The translational implications of these findings might be critical. It is technically straightforward to collect blood from human patients before, during, and after drug treatment. This is not routinely done at the moment. The ability to obtain T cell repertoire data from these samples is, at least technically, straightforward as well. If we are able to translate our findings here, of an indication available from these T cell repertoire data into an indication available from human data, that could provide the physician with an additional layer of reconnaissance, informing that in spite of tumor progression, T cell response is still at full strength. Decisions regarding treatment might need to be re-evaluated.

Limitations of the study

Although the study design included responders and non-responders, the final results showed that all mice presented complete response. Although our initial goal has been the stratification of responders and non-responders, this complete response led to two outcomes: (1) a limited number of tumors to work with (three out of the control group; two out of the treated group) and (2) the impossibility to contrast responders and non-responders. Additionally, the small number of available tumors prevented the follow-up of TIL repertoire with peripheral blood repertoire. Another limitation is inherent to the difference between a strain of mice and the heterogeneity of human samples and human phenotypes. The distances between repertoires of the same strain are not expected to represent the distances between individual patients.

Despite the above-mentioned limitations, we believe that we have demonstrated response-related repertoire metrics. This, together with the temporal nature of our data, is the result presented in the article.

Resource availability

Lead contact

Further information and requests for resources and reagents should be directed to and will be fulfilled by the Lead Contact, Sol Efroni (sol.efroni@biu.ac.il).

Materials availability

The syngeneic mice model used in this study was generated by the Charles River Discovery Research Services in Germany, Study Number: P559A1, Experiment Number: S006. We did not generate any unique reagents throughout the current study.

Data and code availability

The raw data reported and analyzed in this article have been deposited in the Sequence Read Archive in National Center for Biotechnology Information (NCBI) under the BioProject accession number "NCBI: PRJNA658348". The code used in this study is available from the corresponding author, Sol Efroni (sol.efroni@biu.ac.il).

METHODS

All methods can be found in the accompanying Transparent Methods supplemental file.

SUPPLEMENTAL INFORMATION

Supplemental Information can be found online at https://doi.org/10.1016/j.isci.2021.102100.

ACKNOWLEDGMENTS

This research was supported in part by Israel Science Foundation, grant number 582/19, and by the Binational Science Foundation, grant 2019090. MS is supported by the Ministry of Science and Higher Education of the Russian Federation grant No. 075-15-2019-1789

AUTHOR CONTRIBUTION

A.Z., M.G., and S.E. designed the study. H.P., T.S., and M.S. analyzed the data. S.E. supervised the study. All authors contributed to the interpretation of the results and writing the manuscript.

DECLARATION OF INTERESTS

The authors declare no competing interests.

Received: September 10, 2020
Revised: November 2, 2020
Accepted: January 20, 2021
Published: February 19, 2021

REFERENCES

Beer, R., Wutzler, P., Gangler, P., and Pfister, W. (1988). Comparative biological and microbiological testing of root canal filling materials. Zahn Mund Kieferheilkd Zentralbl *76*, 473–481.

Benichou, J., Ben-Hamo, R., Louzoun, Y., and Efroni, S. (2012). Rep-Seq: uncovering the immunological repertoire through next-generation sequencing. Immunology *135*, 183–191.

Bolotin, D.A., Poslavsky, S., Mitrophanov, I., Shugay, M., Mamedov, I.Z., Putintseva, E.V., and Chudakov, D.M. (2015). MiXCR: software for comprehensive adaptive immunity profiling. Nat. Methods *12*, 380–381.

Cha, E., Klinger, M., Hou, Y., Cummings, C., Ribas, A., Faham, M., and Fong, L. (2014). Improved survival with T cell clonotype stability after anti-CTLA-4 treatment in cancer patients. Sci. Transl. Med. *6*, 238ra270.

Cha, S.W., Bonissone, S., Na, S., Pevzner, P.A., and Bafna, V. (2017). The antibody repertoire of colorectal cancer. Mol. Cell Proteomics *16*, 2111–2124.

Covacu, R., Philip, H., Jaronen, M., Almeida, J., Kenison, J.E., Darko, S., Chao, C.C., Yaari, G., Louzoun, Y., Carmel, L., et al. (2016). System-wide analysis of the T cell response. Cell Rep. *14*, 2733–2744.

Field, C.S., Hunn, M.K., Ferguson, P.M., Ruedl, C., Ancelet, L.R., and Hermans, I.F. (2017). Blocking CTLA-4 while priming with a whole cell vaccine reshapes the oligoclonal T cell infiltrate and eradicates tumors in an orthotopic glioma model. Oncoimmunology *7*, e1376154.

Friese, C., Harbst, K., Borch, T.H., Westergaard, M.C.W., Pedersen, M., Kverneland, A., Jonsson, G., Donia, M., Svane, I.M., and Met, O. (2020). CTLA-4 blockade boosts the expansion of tumor-reactive CD8(+) tumor-infiltrating lymphocytes in ovarian cancer. Sci. Rep. *10*, 3914.

Galon, J., Costes, A., Sanchez-Cabo, F., Kirilovsky, A., Mlecnik, B., Lagorce-Pages, C., Tosolini, M., Camus, M., Berger, A., Wind, P., et al. (2006). Type, density, and location of immune cells within human colorectal tumors predict clinical outcome. Science *313*, 1960–1964.

Galon, J., Fridman, W.H., and Pages, F. (2007). The adaptive immunologic microenvironment in colorectal cancer: a novel perspective. Cancer Res. *67*, 1883–1886.

Ganesh, K., Stadler, Z.K., Cercek, A., Mendelsohn, R.B., Shia, J., Segal, N.H., and Diaz, L.A., Jr. (2019). Immunotherapy in colorectal cancer: rationale, challenges and potential. Nat. Rev. Gastroenterol. Hepatol. *16*, 361–375.

Godfrey, D.I., Koay, H.F., McCluskey, J., and Gherardin, N.A. (2019). The biology and functional importance of MAIT cells. Nat. Immunol. *20*, 1110–1128.

Gumperz, J.E., Miyake, S., Yamamura, T., and Brenner, M.B. (2002). Functionally distinct subsets of CD1d-restricted natural killer T cells revealed by CD1d tetramer staining. J. Exp. Med. *195*, 625–636.

Harjunpaa, H., and Guillerey, C. (2020). TIGIT as an emerging immune checkpoint. Clin. Exp. Immunol. *200*, 108–119.

He, Y., Cao, J., Zhao, C., Li, X., Zhou, C., and Hirsch, F.R. (2018). TIM-3, a promising target for cancer immunotherapy. Onco Targets Ther. *11*, 7005–7009.

Hosoi, A., Takeda, K., Nagaoka, K., Iino, T., Matsushita, H., Ueha, S., Aoki, S., Matsushima, K., Kubo, M., Morikawa, T., et al. (2018). Increased diversity with reduced "diversity evenness" of tumor infiltrating T-cells for the successful cancer immunotherapy. Sci. Rep. *8*, 1058.

Kronenberg, M. (2014). When less is more: T lymphocyte populations with restricted antigen receptor diversity. J. Immunol. *193*, 975–976.

Leach, D.R., Krummel, M.F., and Allison, J.P. (1996). Enhancement of antitumor immunity by CTLA-4 blockade. Science *271*, 1734–1736.

Li, H., Ye, C., Ji, G., and Han, J. (2012). Determinants of public T cell responses. Cell Res. *22*, 33–42.

Long, L., Zhang, X., Chen, F., Pan, Q., Phiphatwatchara, P., Zeng, Y., and Chen, H. (2018). The promising immune checkpoint LAG-3: from tumor microenvironment to cancer immunotherapy. Genes Cancer *9*, 176–189.

Matsuda, T., Miyauchi, E., Hsu, Y.W., Nagayama, S., Kiyotani, K., Zewde, M., Park, J.H., Kato, T., Harada, M., Matsui, S., et al. (2019). TCR sequencing analysis of cancer tissues and tumor draining lymph nodes in colorectal cancer patients. Oncoimmunology *8*, e1588085.

McDermott, J., and Jimeno, A. (2015). Pembrolizumab: PD-1 inhibition as a therapeutic strategy in cancer. Drugs Today (Barc) *51*, 7–20.

Oh, D.Y., Cham, J., Zhang, L., Fong, G., Kwek, S.S., Klinger, M., Faham, M., and Fong, L. (2017). Immune toxicities elicted by CTLA-4 blockade in cancer patients are associated with early diversification of the T-cell repertoire. Cancer Res. *77*, 1322–1330.

Pai, C.S., Huang, J.T., Lu, X., Simons, D.M., Park, C., Chang, A., Tamaki, W., Liu, E., Roybal, K.T., Seagal, J., et al. (2019). Clonal deletion of tumor-specific T cells by interferon-gamma confers therapeutic resistance to combination immune checkpoint blockade. Immunity *50*, 477–492 e478.

Pallocca, M., Angeli, D., Palombo, F., Sperati, F., Milella, M., Goeman, F., De Nicola, F., Fanciulli, M., Nistico, P., Quintarelli, C., et al. (2019). Combinations of immuno-checkpoint inhibitors predictive biomarkers only marginally improve their individual accuracy. J. Transl. Med. *17*, 131.

Patel, N.P., Guan, P., Bahal, D., Hashem, T., Scheuplein, F., Schaub, R., Nichols, K.E., and Das, R. (2020). Cancer immunotherapeutic potential of NKTT320, a novel, invariant, natural killer T cell-activating, humanized monoclonal antibody. Int. J. Mol. Sci. *21*, 4317.

Pogorelyy, M.V., and Shugay, M. (2019). A framework for annotation of antigen specificities in high-throughput T-cell repertoire sequencing studies. Front. Immunol. *10*, 2159.

Postow, M.A., Callahan, M.K., and Wolchok, J.D. (2015). Immune checkpoint blockade in cancer therapy. J. Clin. Oncol. *33*, 1974–1982.

Quigley, M.F., Greenaway, H.Y., Venturi, V., Lindsay, R., Quinn, K.M., Seder, R.A., Douek, D.C., Davenport, M.P., and Price, D.A. (2010). Convergent recombination shapes the clonotypic landscape of the naive T-cell repertoire. Proc. Natl. Acad. Sci. U S A *107*, 19414–19419.

Rempala, G.A., and Seweryn, M. (2013). Methods for diversity and overlap analysis in T-cell receptor populations. J. Math. Biol. *67*, 1339–1368.

Ritvo, P.G., Saadawi, A., Barennes, P., Quiniou, V., Chaara, W., El Soufi, K., Bonnet, B., Six, A., Shugay, M., Mariotti-Ferrandiz, E., et al. (2018). High-resolution repertoire analysis reveals a major bystander activation of Tfh and Tfr cells. Proc. Natl. Acad. Sci. U S A *115*, 9604–9609.

Robert, L., Tsoi, J., Wang, X., Emerson, R., Homet, B., Chodon, T., Mok, S., Huang, R.R., Cochran, A.J., Comin-Anduix, B., et al. (2014). CTLA4 blockade broadens the peripheral T-cell receptor repertoire. Clin. Cancer Res. *20*, 2424–2432.

Rosati, E., Dowds, C.M., Liaskou, E., Henriksen, E.K.K., Karlsen, T.H., and Franke, A. (2017). Overview of methodologies for T-cell receptor repertoire analysis. BMC Biotechnol. *17*, 61.

Rowshanravan, B., Halliday, N., and Sansom, D.M. (2018). CTLA-4: a moving target in immunotherapy. Blood *131*, 58–67.

Rubelt, F., Busse, C.E., Bukhari, S.A.C., Burckert, J.P., Mariotti-Ferrandiz, E., Cowell, L.G., Watson, C.T., Marthandan, N., Faison, W.J., Hershberg, U., et al. (2017). Adaptive Immune Receptor Repertoire Community recommendations for sharing immune-repertoire sequencing data. Nat. Immunol. *18*, 1274–1278.

Sharma, P., Hu-Lieskovan, S., Wargo, J.A., and Ribas, A. (2017). Primary, adaptive, and acquired resistance to cancer immunotherapy. Cell *168*, 707–723.

Sherwood, A.M., Emerson, R.O., Scherer, D., Habermann, N., Buck, K., Staffa, J., Desmarais, C., Halama, N., Jaeger, D., Schirmacher, P., et al. (2013). Tumor-infiltrating lymphocytes in colorectal tumors display a diversity of T cell receptor sequences that differ from the T cells in adjacent mucosal tissue. Cancer Immunol. Immunother. *62*, 1453–1461.

Simpson, T.R., Li, F., Montalvo-Ortiz, W., Sepulveda, M.A., Bergerhoff, K., Arce, F., Roddie, C., Henry, J.Y., Yagita, H., Wolchok, J.D., et al. (2013). Fc-dependent depletion of tumor-infiltrating regulatory T cells co-defines the efficacy of anti-CTLA-4 therapy against melanoma. J. Exp. Med. *210*, 1695–1710.

Smyth, M.J., Thia, K.Y., Street, S.E., Cretney, E., Trapani, J.A., Taniguchi, M., Kawano, T., Pelikan, S.B., Crowe, N.Y., and Godfrey, D.I. (2000). Differential tumor surveillance by natural killer (NK) and NKT cells. J. Exp. Med. *191*, 661–668.

Snir, T., and Efroni, S. (2020). T cell repertoire sequencing as a cancer's liquid biopsy—can we decode what the immune system is coding? Curr. Opin. Syst. Biol. *24*, 135–141.

Subudhi, S.K., Aparicio, A., Gao, J., Zurita, A.J., Araujo, J.C., Logothetis, C.J., Tahir, S.A., Korivi, B.R., Slack, R.S., Vence, L., et al. (2016). Clonal expansion of CD8 T cells in the systemic circulation precedes development of ipilimumab-induced toxicities. Proc. Natl. Acad. Sci. U S A *113*, 11919–11924.

Tang, J., Shalabi, A., and Hubbard-Lucey, V.M. (2018). Comprehensive analysis of the clinical immuno-oncology landscape. Ann. Oncol. *29*, 84–91.

Treiner, E., Duban, L., Bahram, S., Radosavljevic, M., Wanner, V., Tilloy, F., Affaticati, P., Gilfillan, S., and Lantz, O. (2003). Selection of evolutionarily conserved mucosal-associated invariant T cells by MR1. Nature *422*, 164–169.

Valpione, S., Galvani, E., Tweedy, J., Mundra, P.A., Banyard, A., Middlehurst, P., Barry, J., Mills, S., Salih, Z., Weightman, J., et al. (2020). Immune-awakening revealed by peripheral T cell dynamics after one cycle of immunotherapy. Nat. Cancer *1*, 210–221.

Van Rhijn, I., and Moody, D.B. (2015). Donor unrestricted T cells: a shared human T cell response. J. Immunol. *195*, 1927–1932.

Venturi, V., Price, D.A., Douek, D.C., and Davenport, M.P. (2008). The molecular basis for public T-cell responses? Nat. Rev. Immunol. *8*, 231–238.

Yamashita, K., Arimoto, A., Nishi, M., Tanaka, T., Fujita, M., Fukuoka, E., Sugita, Y., Nakagawa, A., Hasegawa, H., Suzuki, S., et al. (2018). Application of iNKT cell-targeted active immunotherapy in cancer treatment. Anticancer Res. *38*, 4233–4239.

Zhang, Y., Zheng, L., Zhang, L., Hu, X., Ren, X., and Zhang, Z. (2019). Deep single-cell RNA sequencing data of individual T cells from treatment-naive colorectal cancer patients. Sci. Data *6*, 131.

iScience, Volume *24*

Supplemental Information

A T cell repertoire timestamp is at the core of responsiveness to CTLA-4 blockade

Hagit Philip, Tom Snir, Miri Gordin, Mikhail Shugay, Alona Zilberberg, and Sol Efroni

Supplemental Information

Supplemental Figures and Legends

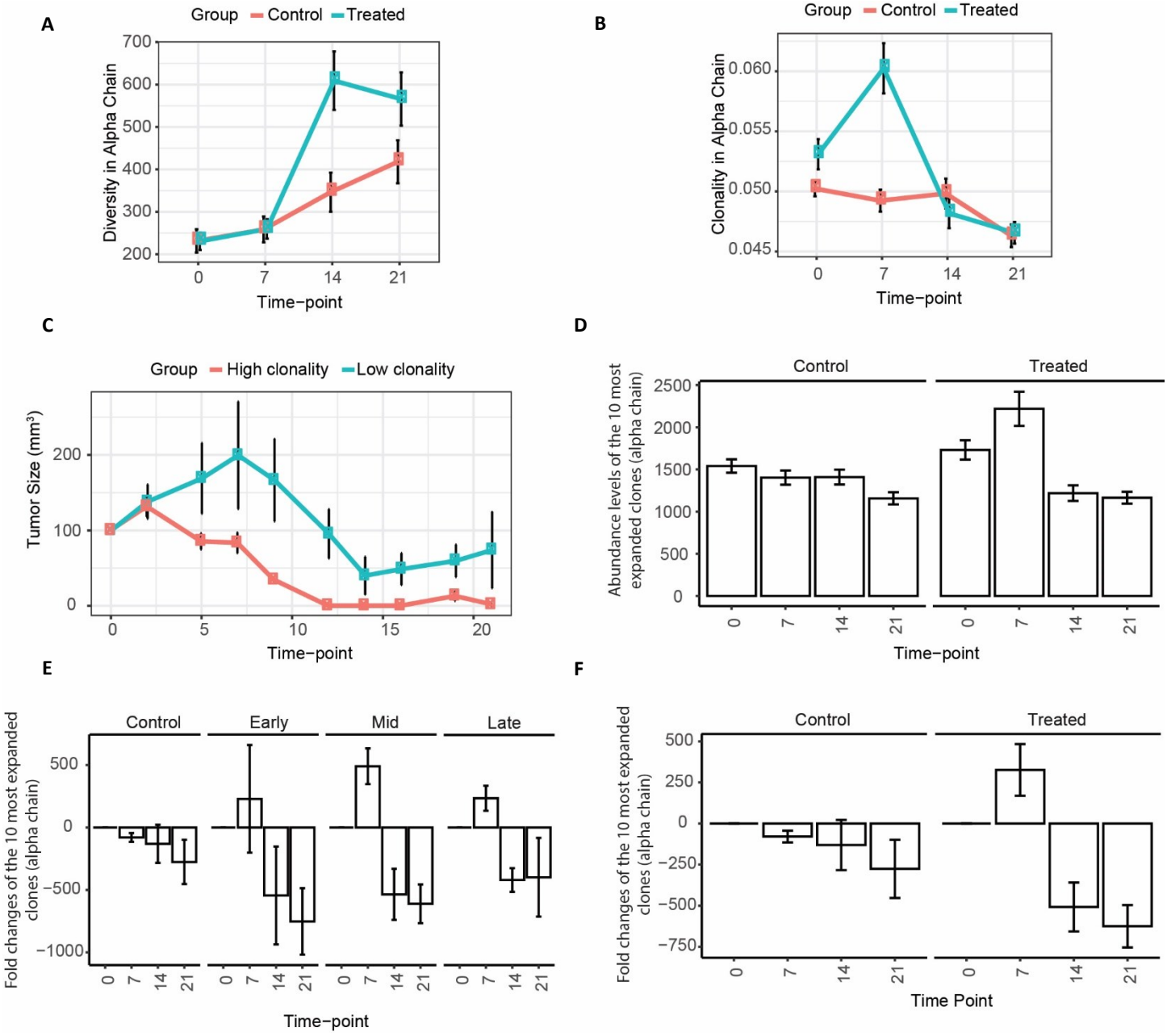

Figure S1. Changes in clonality and diversity in alpha chain, related to Figure 2.

The changes over time in diversity index **(A),** and clonality index **(B)** for alpha chain in the control group and in the treated group. **(C)** The changes over time in the average tumor size. The treated mice in this panel are divided into two groups, according to their clonality index in the alpha chain – low clonality (blue lines) and high clonality (orange lines). **(D)** The abundance levels (copy number) of the 10 most expanded clones in the control and treated groups in an amino-acid view, in alpha chain **(E)** Fold changes of the 10 most abundant clones in alpha chain, when animals are stratified into response groups (early, mid, late, see text) and **(F)** combined. Data of all panels are represented as mean ± SEM.

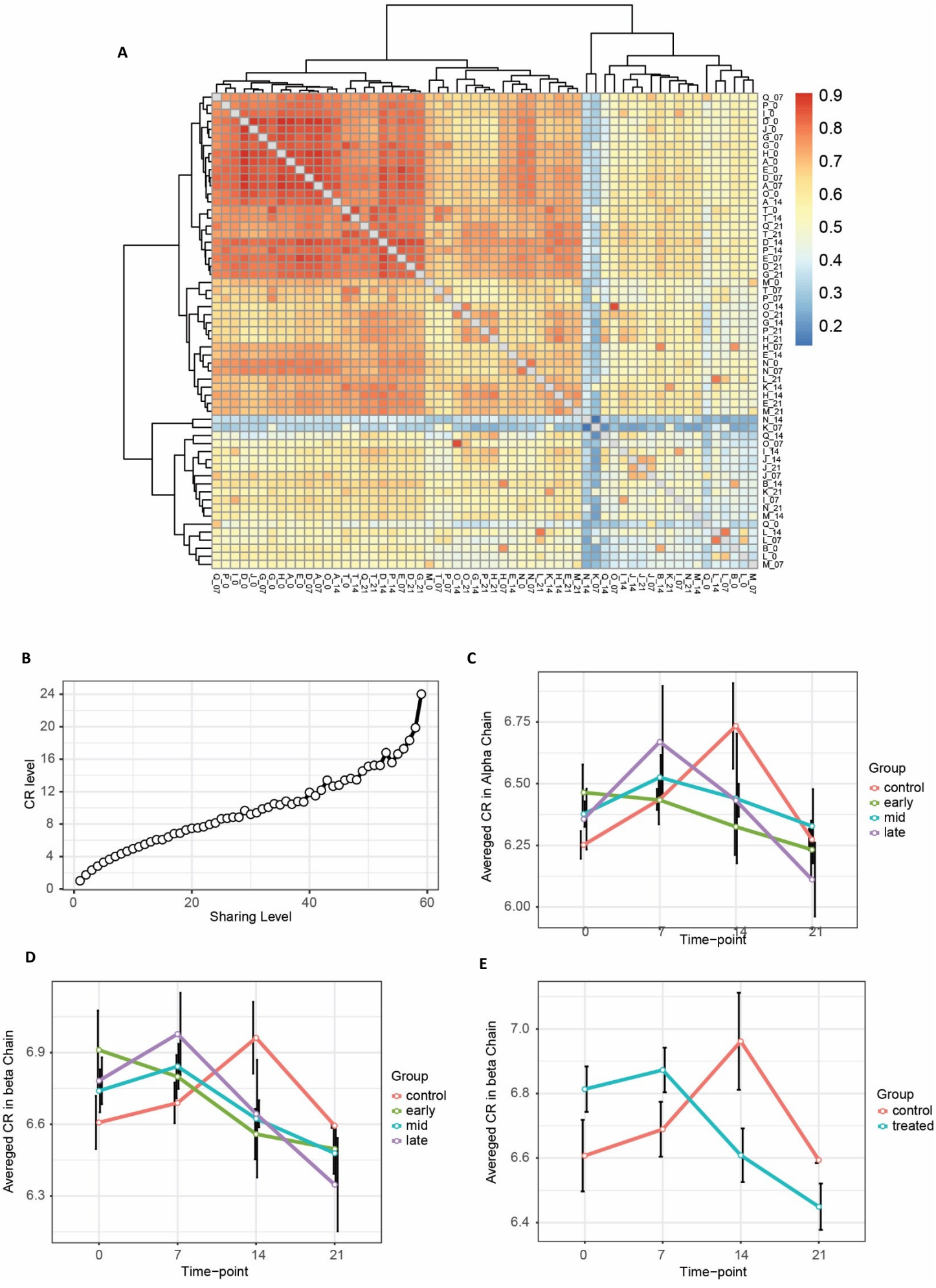
A
0.9
0.8
0.7
0.6
0.5
0.4
0.3
0.2
B
CR level
Sharing Level
C
Avereged CR in Alpha Chain
Time−point
Group
control
early
mid
late
D
Avereged CR in beta Chain
Time−point
Group
control
early
mid
late
E
Avereged CR in beta Chain
Time−point
Group
control
treated

Figure S2. Repertoire dependent response to treatment, Related to Figure 3.

(A) Overlaps between samples in alpha chain. We used the 100 most abundant clones in each sample for the calculation. The metric we used is Morisita's index. The panel shows the inner similarity within samples of the same animal. **(B)** A scatter plot of the co-behavior of sharing levels and the CR level. Sharing level is calculated as the number of samples in which this specific sequence appears. The sequence is the AA sequence of the CDR3. **(C, D)** Changes over time in the averaged CR levels in the different groups in alpha (C) and beta (D) chains. Data are represented as mean ± SEM. **(E)** Changes over time in the averaged CR levels in control and treated groups in beta chain. Data are represented as mean ± SEM.

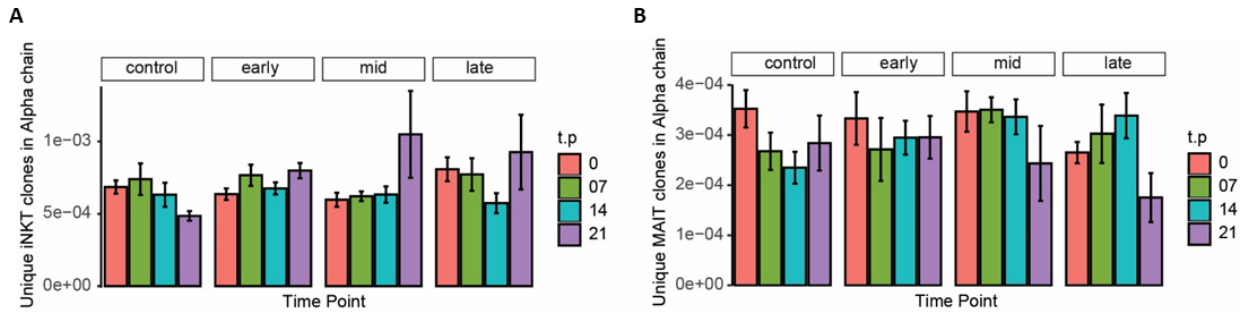

Figure S3. Response and behavior are related to presence of specific TCRs and cell types, Related to Figure 5.

(A) The frequency of iNKT cells in the unique repertoire in alpha chain for all 4 different groups. **(B)** The frequency of MAIT cells in the unique repertoire in alpha chain. Data of all panels are represented as mean ± SEM.

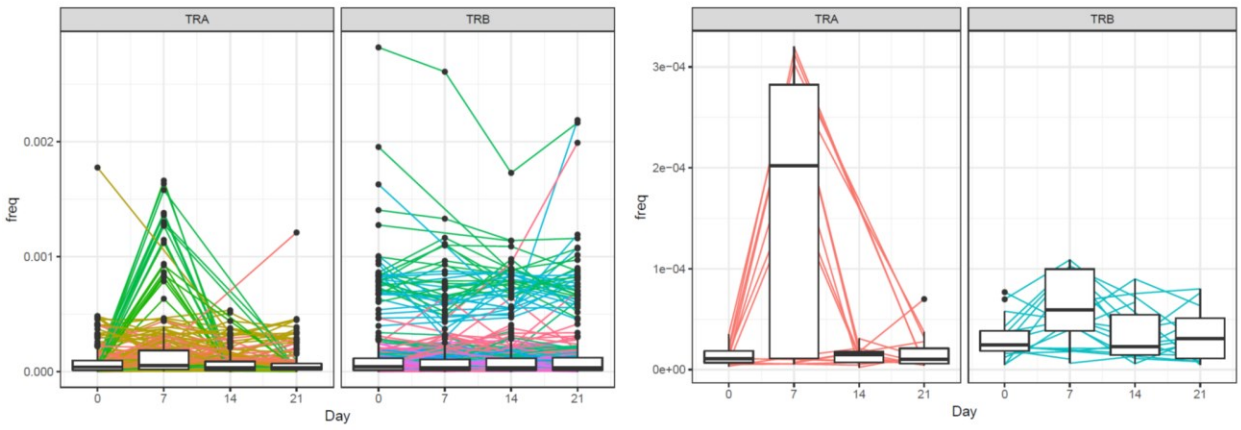

Figure S4. Expression analysis of clonotypes by time points, Related to Figure 6.

Cluster expression is plotted by time points.

Supplemental tables

Control Group											
Abs. Tumor Volume [mm3]	Study Day (After Randomization)										Survival until Day
Date:	**23-Aug-17**	**25-Aug-17**	**28-Aug-17**	**30-Aug-17**	**01-Sep-17**	**04-Sep-17**	**06-Sep-17**	**08-Sep-17**	**11-Sep-17**	**13-Sep-17**	
Animal No	0	2	5	7	9	12	14	16	19	21	
972273000465496R	110.1	199.0	368.8	781.8	936.4	1053.6	1261.0	1956.2			**16***
972273000466396R	87.2	157.3	222.7	362.8	637.2	1097.8	1186.6				**16**
972273000469305R	99.0	143.3	166.2	227.1	227.9	134.2	53.1	27.7	26.4	19.4	**21**
972273000473539R	103.6	149.5	226.3	334.2	354.9	378.7	509.2	542.5	654.5	834.0	**21**
972273000474834R	91.2	105.5	145.8	337.2	406.0	649.0	814.3	1092.7	1213.8	1362.6	**21**
Treated Group											
Abs. Tumor Volume [mm3]	Study Day (After Randomization)										Survival until Day
Date:	**23-Aug-17**	**25-Aug-17**	**28-Aug-17**	**30-Aug-17**	**01-Sep-17**	**04-Sep-17**	**06-Sep-17**	**08-Sep-17**	**11-Sep-17**	**13-Sep-17**	
Animal No	0	2	5	7	9	12	14	16	19	21	
972273000464313R	115.4	305.2	442.7	600.4	400.6	401.2	203.9	108.7	122.4	48.7	**21**
972273000464346R	88.8	87.0	103.2	78.3	26.3	0.1	0.1	0.1	0.1	0.1	**21**
972273000465704R	90.3	130.3	73.9	91.9	39.2	0.1	0.1	0.1	11.1	0.1	**21**
972273000465996R	110.1	167.8	92.7	55.8	46.7	0.1	0.1	0.1	0.1	0.1	**21**
972273000466044R	85.1	170.6	265.6	344.3	256.3	151.4	68.9	69.3	88.5	231.4	**21**
972273000466701R	109.3	187.0	215.2	191.1	180.4	93.5	0.1	22.6	36.8	12.5	**21**
972273000472395R	99.9	184.0	98.7	77.3	34.5	0.1	0.1	0.1	0.1	0.1	**21**
972273000473876R	92.2	63.4	49.5	27.7	23.5	0.1	0.1	24.0	29.1	17.0	**21**
972273000474077R	109.2	112.5	102.9	149.5	32.5	0.1	0.1	0.1	42.0	0.1	**21**
972273000474335R	95.8	104.7	36.0	44.6	27.5	0.1	0.1	0.1	26.0	11.3	**21**
972273000474513R	106.3	106.7	69.8	51.9	19.8	0.1	0.1	34.7	38.9	17.2	**21**

972273000474615R	89.7	147.1	132.5	181.1	31.6	0.1	0.1	21.6	34.0	23.8	**21**
972273000474756R	95.7	109.2	195.3	303.7	263.4	150.7	113.9	110.1	113.4	65.1	**21**
972273000474853R	100.7	169.1	65.4	78.5	60.5	0.1	0.1	0.1	23.2	16.2	**21**
972273000474973R	99.1	135.1	77.8	70.8	65.8	55.6	0.1	0.1	10.5	0.1	**21**

Table S1. Absolute tumor volumes, related to Figure 2.
Mice were routinely monitored at least twice daily on working days and at least once daily on weekends and public holidays.
The absolute tumor volumes (ATVs) were determined by two-dimensional measurement with a caliper on the day of randomization and then three times a week. Tumor volumes were calculated according to the formula described at the results section.

Sequence	sharing
CASSLELGGREQYF	7
CASSPGTGGYEQYF	6
CASSPDRGDTEVFF	5
CASGDSQNTLYF	4
CASSLGGEQYF	4
CASSLRVSNERLFF	4
CASSPSSYEQYF	4
CASSDWGSSYEQYF	3
CASSLDRGDTEVFF	3
CASSLELGGPEQYF	3
CASSLGGNYAEQFF	3
CASSLGQYEQYF	3
CASSLGSSYEQYF	3
CASSPGQANTEVFF	3
CASSQEQGGAETLYF	3
CASSQGQANTEVFF	3
CASSRDNYAEQFF	3
CASSSGTGGYEQYF	3

Table S2. Abundant clones identified in the treated mice, Related to Figure 5.

Clones that are in the top 100 clones at day 7 and are shared among at least two time points of the same animal. The sharing level represents the number of different mice that answer this definition (top clone in day 7 and sharing >= 2).

mouse	group
A	control
B	control
C	control
D	control
E	control
F	Late-responders
G	Late-responders
H	Late-responders
I	Late-responders
J	Mid-responders
K	Late-responders
L	Early-responders
M	Mid-responders
N	Early-responders
O	Mid-responders
P	Early-responders
Q	Early-responders
R	Early-responders
S	Mid-responders
T	Mid-responders

Table S3. Mice response to treatment, Related to the Transparent Methods.

The categories of the different mice according to their response to treatment: control, early-responders, mid-responders and late-responders.

TRANSPARENT METHODS

Mice and experiment procedure

The study comprises of a single efficacy experiment with the syngeneic mouse tumor model MC38. $5 \cdot 10^5$ MC38 cells, which were derived from a chemically induced grade III mouse colon adenocarcinoma were subcutaneously implanted into immunocompetent C57BL/6N mice (Strain C57Bl/6NAnNCrl, Charles River). The experiment contained 2 groups, of which the first group (5 animals) was dosed with 10 ml/kg/day of vehicle on day 1, 3 and 6 of the experiment. The second group (15 animals) was dosed with the investigational antibody anti-mCTLA4 (5/2.5 mg/kg/day at 1/3, 6). After treatment with the immune checkpoint inhibitor antibody anti-mCTLA4 blood samples for the preparation of PBMCs were taken at days 0,7,14 and 21.

General Specifications, Animal Health, Identification

All experiments and protocols were approved by the animal welfare body at CR Discovery Research Services Germany and the local authorities, and were conducted according to all applicable international, national and local laws and guidelines. Only animals with unobjectionable health were selected to enter testing procedures. The animals were delivered at the age of four to six weeks and were used for experiments after at least one week of acclimatization. Animals were arbitrarily numbered during tumor implantation using radio frequency identification transponders. Each cage was labeled with a record card indicating all relevant experimental details.

Housing Conditions

Animals were housed in individually ventilated cages (TECNIPLAST Sealsafe™-IVC-System, TECNIPLAST, Hohenpeissenberg, Germany), depending on group size, either in type III or type II long cages. They were kept under a 14L:10D artificial light cycle. The temperature inside the cages was maintained at 25ºC with a relative humidity of 40-70% and 60-65 air changes/hour in the cage. Dust-free bedding consisting of aspen wood chips with approximate dimensions of 5 x 5 x 1 mm (ABEDD® - LAB & VET Service GmbH, Vienna, Austria, Product Code: LTE E 001) and additional nesting material were used. The cages including the bedding and the nesting material were changed weekly. The animals were fed autoclaved Teklad Global 19% Protein Extruded Diet (T.2019S.12) from Envigo RMS SARL and had access to sterile filtered and acidified (pH 2.5) tap water that was changed twice weekly. Feed and water were provided ad libitum. All materials were autoclaved prior to use.

Immunotherapy treatment

A dosing solution with a concentration of 0.5 mg/ml for dosing at 5 mg/kg/day was freshly prepared on dosing day 1 by dilution of 203 µl of anti-mCTLA4 stock solution with 2797 µl of PBS. A dosing solution with a concentration of 0.25 mg/ml for dosing at 2.5 mg/kg/day was freshly prepared on dosing day 3 and 6 by dilution of 101 µl of anti-mCTLA4 with 2899 µl of PBS. All dosing solutions were administered in a dose volume of 10 ml/kg.

PBMCs purification from blood samples

100µL of Blood was collected by retro-orbital sinus puncture under isoflurane anesthesia. PBMCs were prepared from 100 µl blood by spinning down cells and lysing pellets with ACK lysis buffer (150 mM ammonium chloride, 10 mM potassium bicarbonate, 0.1 mM EDTA, pH 7.2-7.4) to remove erythrocytes. Resulting PBMC were frozen in 10 % DMSO/90 % FCS at 80°C until shipment.

Tumors and Spleens samples

Tumors (where still visible) were collected immediately after euthanasia, and directly transferred to liquid nitrogen (snap-frozen samples). Spleens were collected immediately after euthanasia, and directly transferred to liquid nitrogen (snap-frozen samples).

RNA purification from Blood, tumor and spleen samples

PBMCs samples were thawed and their total RNA content extracted using the RNeasy mini kit (Qiagen). Tumor and spleen samples were thawed, weighted and applied to Trizol (Invitrogen) purification procedure according to manufacture protocol. The obtained RNA product was then evaluated for its integrity value (RIN) to better standardize RNA quality. Next, RNA concentrations were determined by qubit, which provides an accurate method for the quantitation of low abundance RNA samples.

Library preparation

A fixed total RNA concentration of 250ng from each sample was subjected to the SMARTer TCR profiling kit (Takara); first single cDNA strand is synthesized at the first round of reverse transcription, using poly T primer for the 3' end and a smarter oligo (Switching Mechanism at 5' End of RNA Template) for the 5' ends, catalyzed by MMLV-derived SMARTScibe Reverse Transcriptase. By employing 5' RACE-like approach, the SMARTer TCR profiling kit allows to capture complete V(D)J variable regions of TCR alpha and beta chains and in the following step, each fragment was exponentially increased by PCR. On each dsDNA fragment, dedicated adapters containing flow cell-binding sites, P5 and P7, were inserted to allow the enriched library fragments to attach to the cell flow surface. The TCR sequencing library was size-selected and purified using AMPure XP beads. The generated libraries were measured for their DNA concentration by qubit and assessed for their size by Tapestation or Bioanalyzer.

Miseq sequencing

TCR sequencing was performed on an Illumina Miseq sequencer using the 600-cycle Miseq reagent kit v3 (Illumina) with pair-end, 2x300 base pair reads. Library pool molarity was 4nM.

Processing of raw sequencing data

Transforming raw reads to alpha and beta CDR3 sequences was done by using MiXCR, a universal framework that processes big immunome data from raw sequences and output quantitated clonotypes (Bolotin et al., 2015). For the alpha chain we obtained $13 \cdot 10^6$ reads with an average of 171628 copies and

25159 unique amino-acid clones, and for the beta chain we obtained $18.6 \cdot 10^6$ with an average of 245867 copies and 49725 unique amino-acid clones.

In order to avoid bias originating from different sample sizes, we subsampled 97048 sequences from each sample, as the number of clones in the smallest sample.

Groups

We categorized the following groups: Control (mice A-E); Treated (F-T); Early responders (mice L, N, P, Q, R) – mice that showed relatively faster response to treatment; Mid responders – mice that responded later to treatment (mice J, M, O, S, T), and Late responders - mice that responded much later to treatment (mice F, G, H, I, K) – mice that showed relatively slower response to treatment. Table S3 indicates samples according to these categories.

Clonality and diversity

Since different sample sizes cause differences in the unique sequences in a sample, we used clonality and diversity measures to explore the TCR repertoire.

Clonality is defined as 1 − Pielou's eveness.

and diversity is defined as the Inverse Simpson index:

$$\frac{1}{\lambda} = \frac{1}{\sum_{i=1}^{R} p_i^2} = {}^2D$$

Diversity and clonality are frequently used in TCR repertoire analyses. Diversity is used for assessing the number of unique sequences within the TCR repertoire whereas the clonality measure is used for assessing the proportional abundance of the TCR clones.

Convergent recombination

Convergent recombination (Smyth et al.) is the process where multiple recombination events 'converge' to produce the same nucleotide sequence and multiple nucleotide sequences 'converge' to encode the same amino-acid sequence, which results in different TCR sequences generated in differential frequencies during recombination. This process can further contribute to an increased a priori probability of producing specific TCR sequences. The CR mechanism drives the sharing of antigen specific TCRs between multiple individual mice. Here, we define CR level as the number of different NT sequences encoding a specific AA sequence. To calculate the averaged CR of a sample, we measure the CR level for each AA sequence and averaged all the CR levels of the sequences appeared in a specific sample.

Overlaps

For calculating the overlaps between all the sample pairs, we used the 'morisitas.index' function from the tcR package in R.

For the analysis of averaged overlaps between groups, we calculate the number of overlapped clones for all the pairs of samples within a combination of 2 groups. For example, for the averaged overlap of control and early-responders, we calculated all the overlaps between the pairs of samples from control and early-responders and averaged them.

Motif Analysis

VDJtools (Shugay et al., 2015) was used for conversion and pooling of the data, and then manually split into TRA and TRB. TCRNET was used to compute P-values for clonotype degree in pooled samples:

$d_i = \sum_j \mathbf{I}\left[Hamming(CDR3_i, CDR3_j) \leq 1\right]$

Next, the cleaned data is loaded, P-value correction is performed followed by selection of the worst of the two corrected P-values: one that accounts for VJ usage and one that does not. A threshold of

$P_{adj} < 10^{-5} \text{ and } d \geq 3$ is imposed.

Clustering

To perform clustering of motif elements, we first obtain MDS coordinates, which translate to connected component (clusters). Each cluster ID is noted along with its CDR3 amino acid sequence, the representative V/J, a count summary and other relevant metrics (our code is modular to allow several types of analysis). Finally, only clusters with 5 or more unique CDR3s are included in the final analysis. Code used to generate the figure shown here is available upon request.

Supplemental References

Bolotin, D.A., Poslavsky, S., Mitrophanov, I., Shugay, M., Mamedov, I.Z., Putintseva, E.V., and Chudakov, D.M. (2015). MiXCR: software for comprehensive adaptive immunity profiling. Nat Methods *12*, 380-381.

Shugay, M., Bagaev, D.V., Turchaninova, M.A., Bolotin, D.A., Britanova, O.V., Putintseva, E.V., Pogorelyy, M.V., Nazarov, V.I., Zvyagin, I.V., Kirgizova, V.I.*, et al.* (2015). VDJtools: Unifying Post-analysis of T Cell Receptor Repertoires. PLoS Comput Biol *11*, e1004503.

Smyth, M.J., Thia, K.Y., Street, S.E., Cretney, E., Trapani, J.A., Taniguchi, M., Kawano, T., Pelikan, S.B., Crowe, N.Y., and Godfrey, D.I. (2000). Differential tumor surveillance by natural killer (NK) and NKT cells. J Exp Med *191*, 661-668.